RESEARCH

Evaluating the optical and gamma-ray protection properties of bismo-tellurite sodium titanium zinc glasses

H. O. Tekin[1,2] · Y. S. Rammah[3] · M. M. Hessien[4] · Hesham M. H. Zakaly[5,6] · Shams A. M. Issa[6,7]

Abstract

Optical properties and gamma-ray attenuation competence of bismo-tellurite sodium titanium zinc glass samples with chemical formula $(80-x)TeO_2–10ZnO–5TiO_2–5Na_2O–xBi_2O_3$, where $x = 5, 8, 10, 12$, and 15 mol% have been explored. Values of optical electronegativity (χ^*) were varied from 0.715 for B5 glass sample to 0.677 for B15 glass sample. Values of linear dielectric susceptibility ($\chi^{(1)}$) were varied from 0.400 for B5 glass sample to 0.430 for glass sample. Values of non-linear optical susceptibility (χ^3) and non-linear refractive index $\left(n_2^{\text{optical}}\right)$ were varied from 4.379×10^{-12} to 5.812×10^{-12} (esu) and from 6.719×10^{11} to 8.656×10^{-11} (esu) for B5 and B15 glasses, respectively. The B15 sample with the highest Bi_2O_3 content had the maximum mass attenuation coefficient (μ_m) values across all examined photon energies, while B5 sample with the lowest Bi_2O_3 content had the minimum (μ_m). Both half-value layer ($T_{0.5}$) and mean free path (λ) followed the trend as follows: $(T_{0.5}, \lambda)_{B5} > (T_{0.5}, \lambda)_{B8} > (T_{0.5}, \lambda)_{B10} > (T_{0.5}, \lambda)_{B12} > (T_{0.5}, \lambda)_{B15}$. The exposure and energy absorption buildup factor (EBF and EABF) values decrease from B5 to B15, demonstrating that the shielding enhancement of glass samples has strengthened. The effective atomic number (Z_{eff}) parameter followed the trend as follows: $(Z_{eff})_{B15} > (Z_{eff})_{B12} > (Z_{eff})_{B10} > (Z_{eff})_{B8} > (Z_{eff})_{B5}$. Our findings confirm that the enhancement of Bi_2O_3 content in the bismo-tellurite sodium titanium zinc glass samples plays an important role of improvement in both optical and gamma-ray protection properties.

Keywords Bismo-tellurite glasses · Optical electronegativity · Mass attenuation coefficient · EABF

Introduction

The science and technology of radiation shielding is a major factor for the continued growth of nuclear energy applications and facilities around the world. The energy, medical, and research industries are just a few of the many industries that have benefited greatly from the peaceful usage of nuclear energy. Radiation protection technology also aids in assuring the public of the inherent safety of nuclear energy and radiation [1–3]. In general, in all radiation-based technology, the optimization of radiation operations and the limitation of dosage are cardinal objectives in all protective guidelines. These standards were created primarily to safeguard people and the environment from the consequences of uncontrolled radiation exposure [3, 4].

When creating the composition of glass, heavy metal oxides are frequently used in order to enhance the shielding potential of the glass system in question. Adding heavy metal oxides to a glass system can significantly increase the overall density of the glass, which is typically associated with improved shielding ability [5, 6]. Heavy metal oxides

✉ Y. S. Rammah
dr_yasser1974@yahoo.com

1. Department of Medical Diagnostic Imaging, College of Health Sciences, University of Sharjah, 27272 Sharjah, United Arab Emirates

2. Istinye University, Faculty of Engineering and Natural Sciences, Computer Engineering Department, Istinye University, Istanbul 34396, Turkey

3. Department of Physics, Faculty of Science, Menoufia University, Shebin El-Koom 32511, Menoufia, Egypt

4. Department of Chemistry, College of Science, Taif University, P.O. Box 11099, Taif 21974, Saudi Arabia

5. Ural Federal University, Yekaterinburg 620002, Russia

6. Physics Department, Faculty of Science, Al-Azhar University, Assuit 71524, Egypt

7. Department of Physics, Faculty of Science, University of Tabuk, Tabuk, Saudi Arabia

Table 1 Code, chemical composition, and density of the $(80-x)$ $TeO_2–10ZnO–5TiO_2–5Na_2O–xBi_2O_3$, where $x=5$, 8, 10, 12, and 15 mol%

Sample code	Composition (mole %)	Density, ρ (g/cm³)
B5	$75TeO_2–10ZnO–5TiO_2–5Na_2O–5Bi_2O_3$	5.401
B8	$72TeO_2–10ZnO–5TiO_2–5Na_2O–8Bi_2O_3$	5.613
B10	$70TeO_2–10ZnO–5TiO_2–5Na_2O–10Bi_2O_3$	5.762
B12	$68TeO_2–10ZnO–5TiO_2–5Na_2O–12Bi_2O_3$	5.844
B15	$65TeO_2–10ZnO–5TiO_2–5Na_2O–15Bi_2O_3$	6.138

are metal oxides with a high density, and when they are added to a glass system, they can significantly increase the overall density of the glass system. Because of its high density and excellent attenuation capabilities, Bi_2O_3 is a heavy metal oxide that is widely employed [7]. Bi_2O_3 is also frequently utilized as a lead substitute due to the fact that it has qualities that are similar to lead when it comes to radiation shielding. Bi_2O_3 can be used as a glass intermediate in a variety of applications, including glass modification and glass formation, depending on the composition of the glass matrix. Bi_2O_3 is a chemical compound that is used in the production of glass. A glassmaker is responsible for forming the backbone of the glass structure, whereas a glass modifier affects the structure of the glass but does not contribute to its formation as a whole [8, 9].

Borate-based glasses have a wide range of glass forming regions, a low melting point, high thermal stability, strong bond strength, high rare earth ion solubility, smaller cation size, and high transparency [10–16]. It has a random network structure made up of trigonal BO3 units that, depending on the modifier oxide glasses type and concentration, can be transformed into tetrahedral BO4 units [17, 18].

Glasses incorporating alkaline, alkali, rare-earth, and/ or transition metals perform well in a variety of applications [19–23], including solid-state electrolytes [19, 20],

solid-state illumination [21], optoelectronic devices [22], and radiation shielding [24–29].

The objectives of this work are to explore the following interesting characteristics of high dense $TeO_2–ZnO–TiO_2–Na_2O–Bi_2O_3$. In addition to the linear dielectric susceptibility ($\chi^{(1)}$), the electronegativity (χ^*), and the non-linear refractive index ($n_2^{optical}$), the non-linear optical susceptibility (χ^3) is also measured. Using two different tools (MCNPX [30] Monte Carlo simulations and Phy-X/ PSD [31] software), the gamma-ray attenuation competencies of the investigated glasses are evaluated: linear (μ) and mass (μ_m) attenuation coefficients, half-value layer (HVL), effective atomic (Z_{eff}), and exposure and energy absorption buildup factors (EBF and EABF).

Materials

Bismo-tellurite sodium titanium zinc glasses (B5–B15)

Bismo-tellurite sodium titanium zinc glass samples with chemical formula $(80-x)$ $TeO_2–10ZnO–5TiO_2–5Na_2O–xBi_2O_3$, where $x=5$ mol%, 8 mol%, 10 mol%, 12 mol%, and 15 mol% have been synthesized previously via using the conventional melt quenching process [32]. These glasses are selected in order to achieve the aims of this work. The investigated samples are named as (see Table 1):

(i) $75TeO_2-10ZnO-5TiO_2-5Na_2O-5Bi_2O_3$: **B5** with density 5.401 (g/cm³)
(ii) $72TeO_2-10ZnO-5TiO_2-5Na_2O-8Bi_2O_3$: **B8** with density 5.613 (g/cm³)
(iii) $70TeO_2-10ZnO-5TiO_2-5Na_2O-10Bi_2O_3$: **B10** with density 5.762 (g/cm³)

Table 2 $E^{optical}$, $n^{optical}$, (χ^*), ($\chi^{(1)}$), (χ^3), and $\left(n_2^{optical}\right)$ of the B5–B15 studied glasses

Physical parameter	Sample code				
	B5	**B8**	**B10**	**B12**	**B15**
Energy gap, $E^{optical}$ (eV) ± 0.01 [32]	2.66	2.65	2.64	2.59	2.52
Linear refractive index, $n^{optical} \pm 0.001$ [32]	2.456	2.459	2.265	2.520	2.530
Optical electronegativity (χ^*) ± 0.001 P.W*	0.715	0.712	0.709	0.696	0.677
Linear dielectric susceptibility ($\chi^{(1)}$) ± 0.001 P.W*	0.400	0,401	0.404	0.425	0.430
Non-linear optical susceptibility (χ^3) $\times 10^{-12}$ (esu) ± 0.001 P.W*	4.379	4.431	4.535	5.598	5.812
Non-linear refractive index $\left(n_2^{optical}\right) \times 10^{-11}$ (esu) ± 0.001 P.W*	6.719	6.789	6.933	8.370	8.656

$P.W^*$ present work

Fig. 1 Dependence of (**a**) χ^* and (**b**) $\chi^{(1)}$ on Bi_2O_3 concentration mol% of B5–B15 glasses
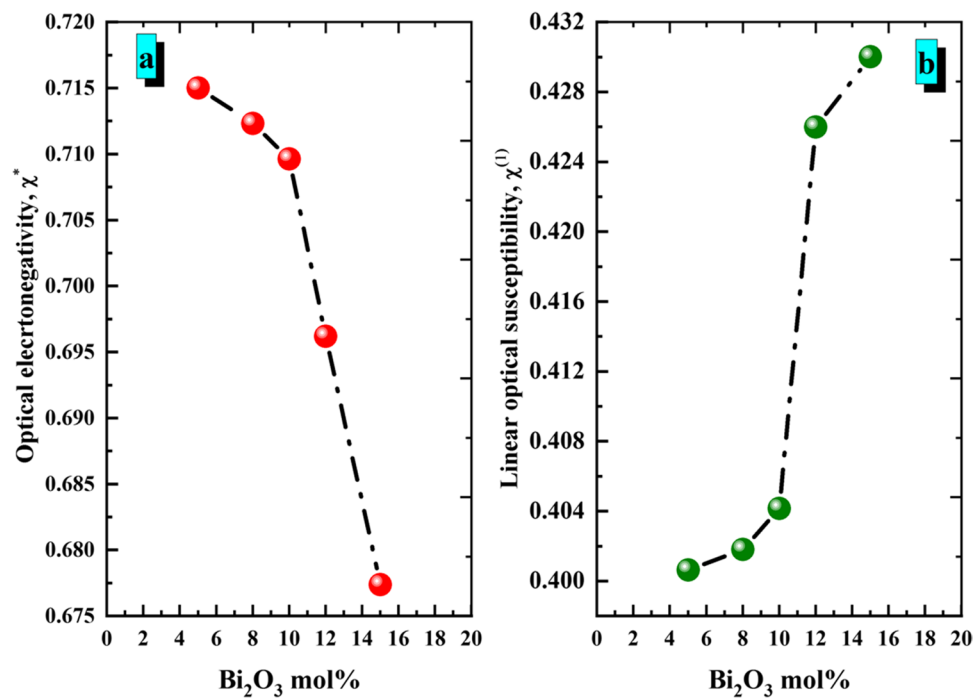
(iv) $68TeO_2$-$10ZnO$-$5TiO_2$-$5Na_2O$-$12Bi_2O_3$: **B12** with density 5.844 (g/cm^3)

(v) $65TeO_2$-$10ZnO$-$5TiO_2$-$5Na_2O$-$15Bi_2O_3$: **B15** with density 6.138 (g/cm^3)

Results and discussion

Optical properties of B5–B15 glasses

These glasses (B5–B15), which were evaluated in this study, were found to have high electronegativity and low linear dielectric susceptibility ($\chi^{(1)}$), which were measured.

Fig. 2 Dependence of (**a**) χ^3 and (**b**) $n_2^{optical}$ on Bi_2O_3 concentration mol% of B5–B15 glasses
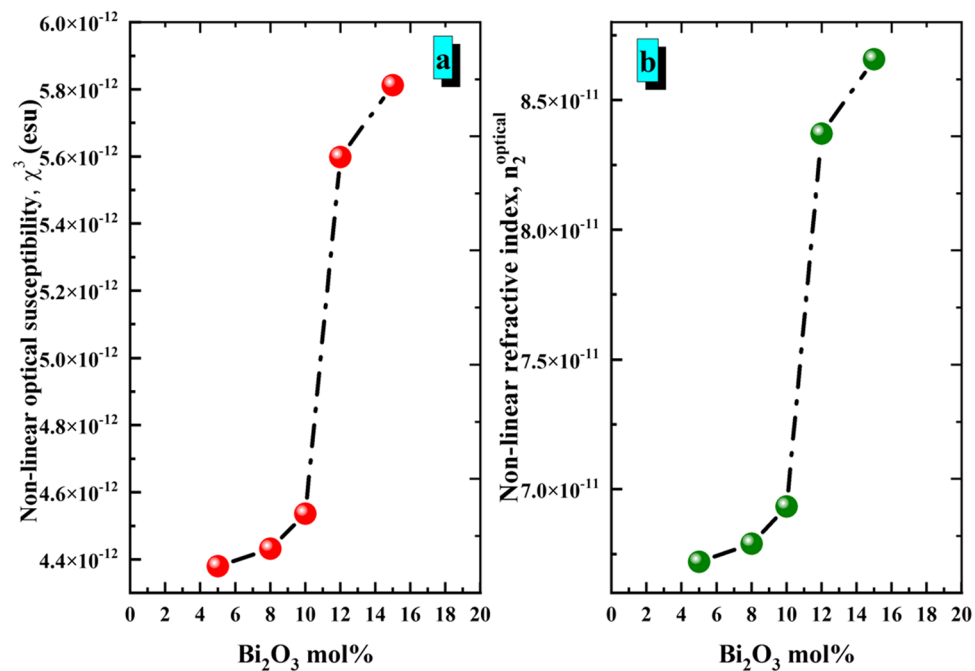
Fig. 3 Variation of glass densities (g/cm³)
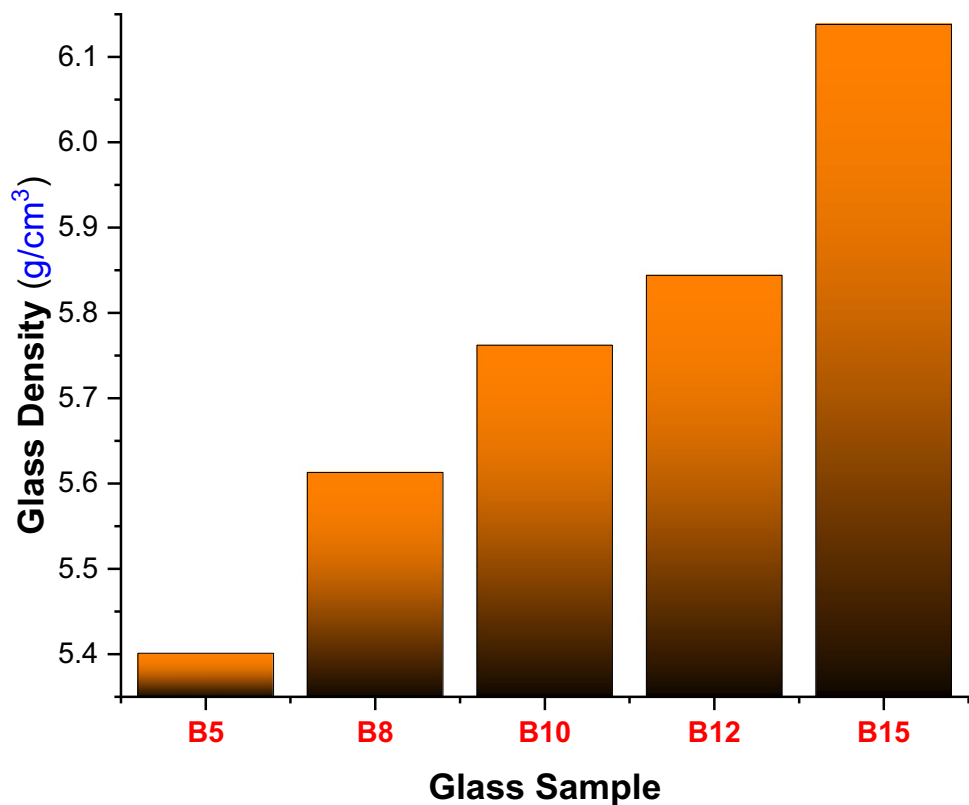

The electronegativity (χ^*) of a cation and an anion can be computed with the help of the electronegativity of the cation. Duffy [33] has proposed a relationship to find the χ^* for complicated systems like the one under investigation

Fig. 4 Variation of mass attenuation coefficients (cm²/g) of investigated glasses as a function of incident photon energy (MeV)
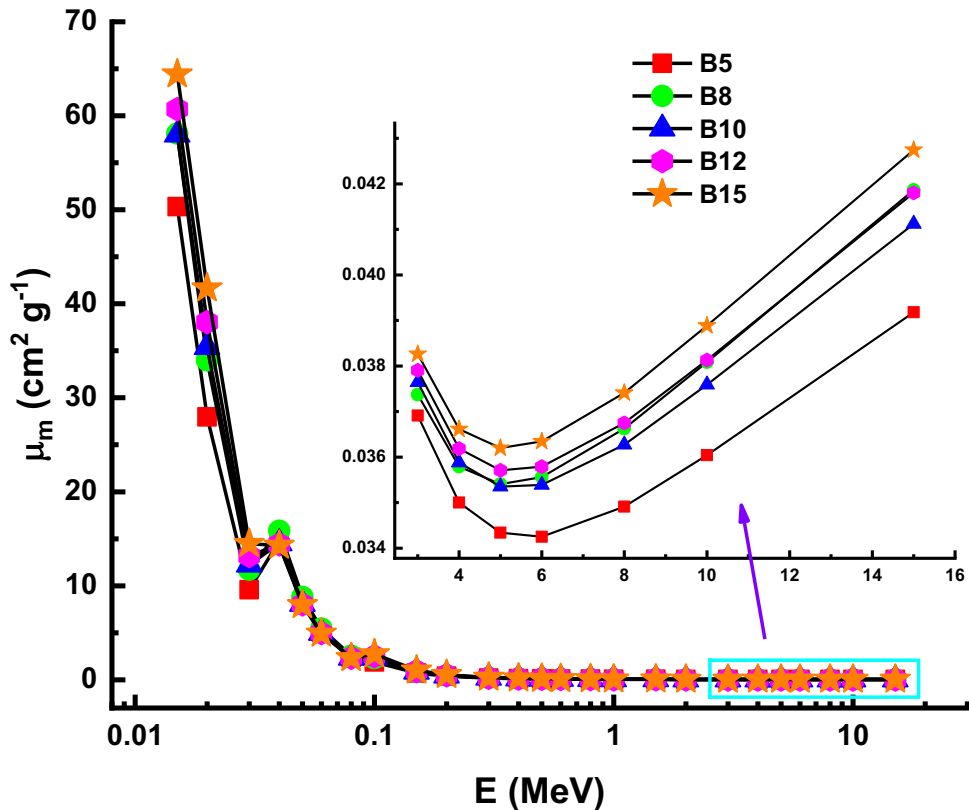
Fig. 5 Variation of half-value layer (cm) values of investigated glasses as a function of incident photon energy (MeV)
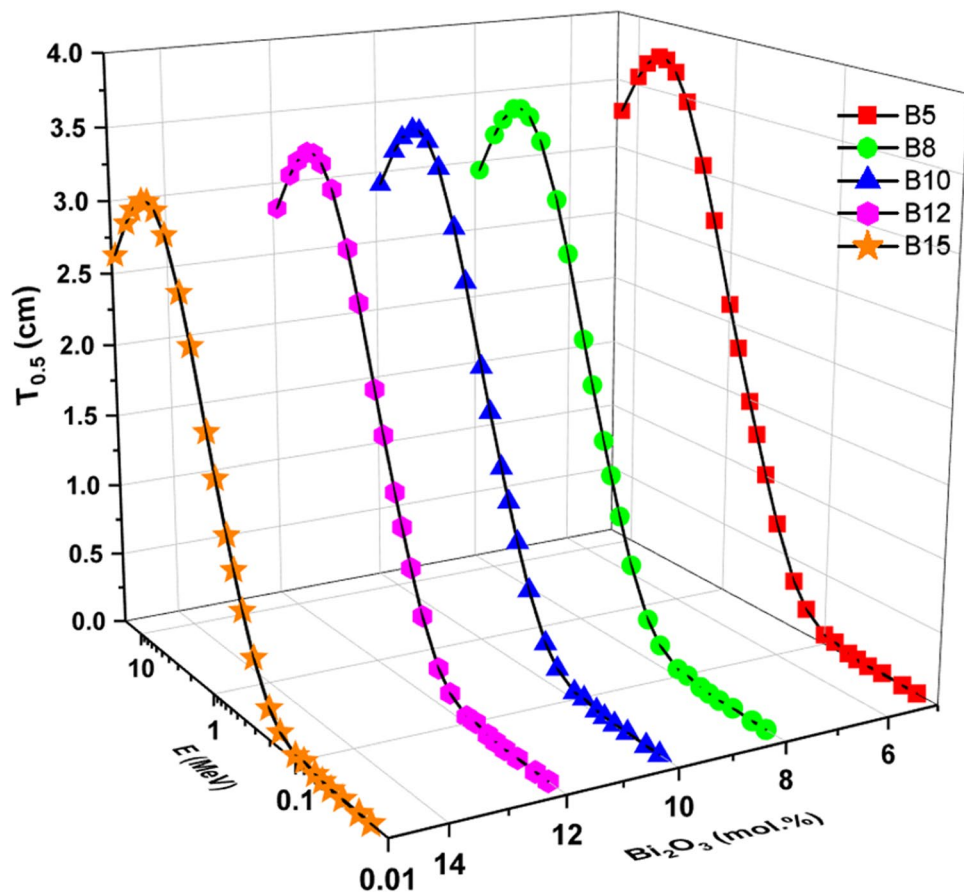
Fig. 6 Variation of mean free path (cm) values of investigated glasses as a function of incident photon energy (MeV)
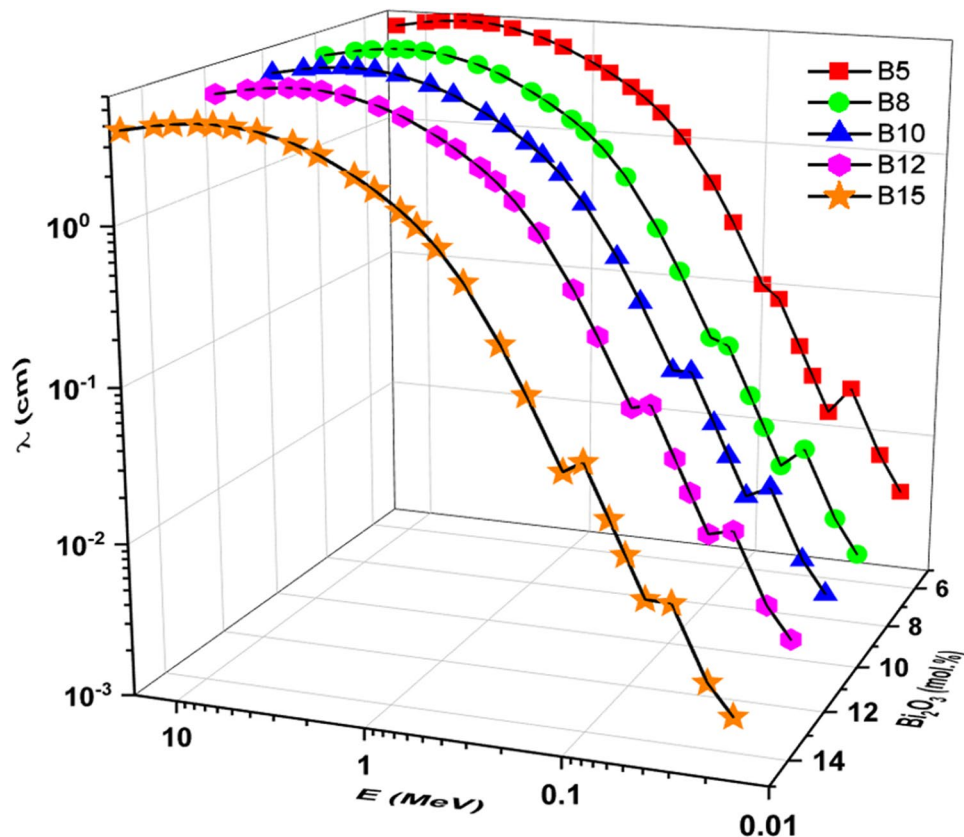
$(B_2O_3–TeO_2–TiO_2–Na_2O–ZnO)$, which is depicted in Eq. (1). Additionally,

$$\chi^* = 0.2688 E^{optical} \tag{1}$$

where $E^{optical}$ is the optical energy bandgap. The values of $E^{optival}$ of B5–B15 glasses are listed in Table 2 [32]. When it comes to glasses, the linear dielectric susceptibility ($\chi^{(1)}$) is a characteristic that analyzes a material's ability to become totally polarized. The following Eq. (2) can be used to compute the $\chi^{(1)}$ of glasses [33, 34]:

$$\chi^{(1)} = \left(\left(n_2^{optical} \right)^2 - 1 \right)/4\pi \tag{2}$$

where $n^{optical}$ is the linear optical refractive index. Values of $n^{optical}$ of B5–B15 glasses are listed in Table 2 [32]. Figure 1a and b depict the variation of the χ^* and $\chi^{(1)}$ with Bi_2O_3 content in the investigated B5–B15 samples. As seen in Fig. 1a and b, the values of χ^* and $\chi^{(1)}$ have an opposite trend. Therefore, behaviors of the χ^* and $\chi^{(1)}$ can be discussed as the modifications in the structure of B5–B15 glasses with adding of Bi_2O_3 helps to change the number of non-bridging oxygen (NBO) in the network structure [32].

The non-linear refractive index $\left(n_2^{optical} \right)$ and non-linear optical susceptibility (χ^3)) of the investigated B5–B15 glasses were calculated via Ticha and Tichy postulation [35]:

$$\chi^3(esu) = A/(4\pi)^4 (n^{optical} - 1)^4 \tag{3}$$

$$n_n^{optical}(esu) = \frac{12\pi \chi^3}{n^{optical}} \tag{4}$$

where $A = 1.7 \times 10^{-10}$ is a constant. Values of the calculated $\chi^{(3)}$ and $n_2^{optical}$ for the investigated B5–B15 glasses are plotted as a function of Bi_2O_3 content in Fig. 2a and b, respectively. Also, values of $\chi^{(3)}$ and $n_2^{optical}$ are listed in Table 2. From Fig. 2a and b, it was seen that two non-linear optical parameters have a similar trend of the investigated glasses; this may be attributed to the increasing in the non-bridging oxygen (NBO) in glass structures [32].

Radiation protection properties of B5–B15 glasses

In this study, radiation shielding properties of five different glass samples (B5–B15) based on

Fig. 7 Variation of effective atomic number (Z_{eff}) values of investigated glasses as a function of incident photon energy (MeV)
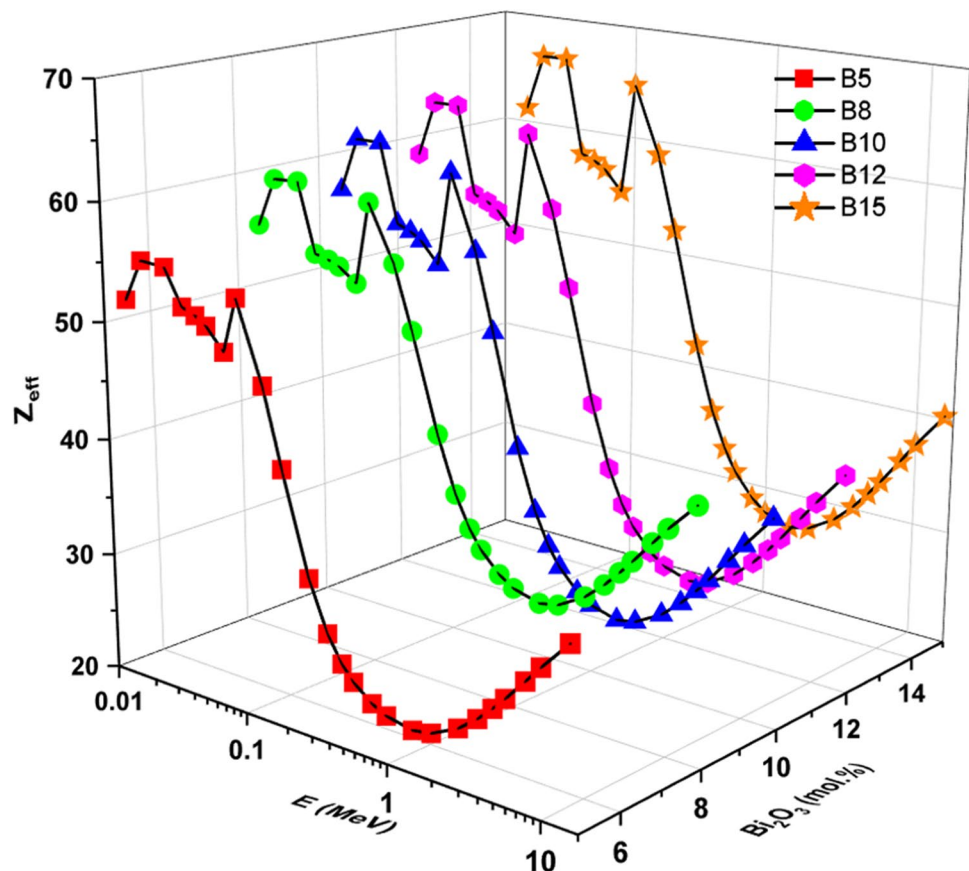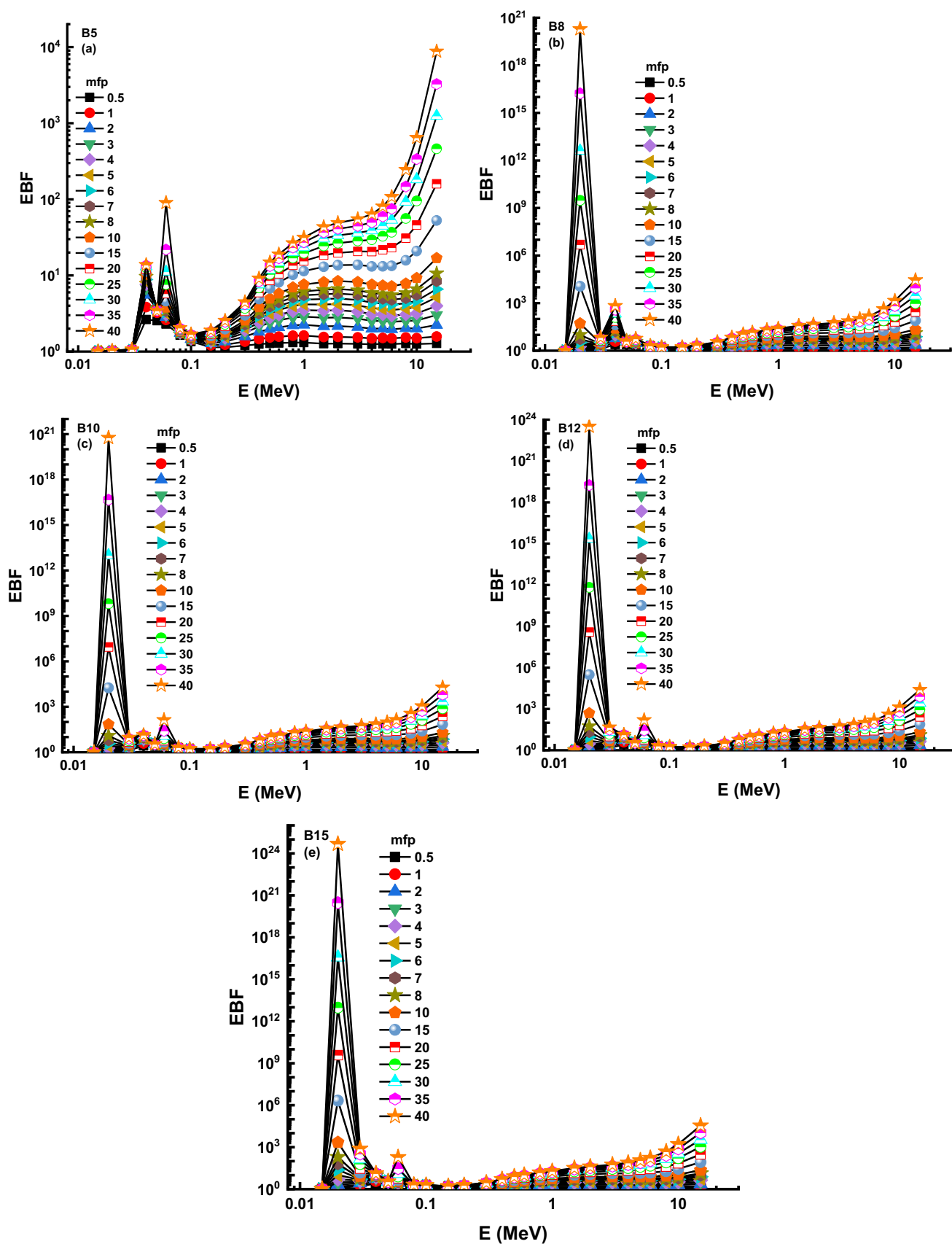
Fig. 8 Variation of exposure buildup factor (EBF) values of glasses at different MFP values (from 0.5 to 40 MFP) as a function of incident photon energy (MeV)
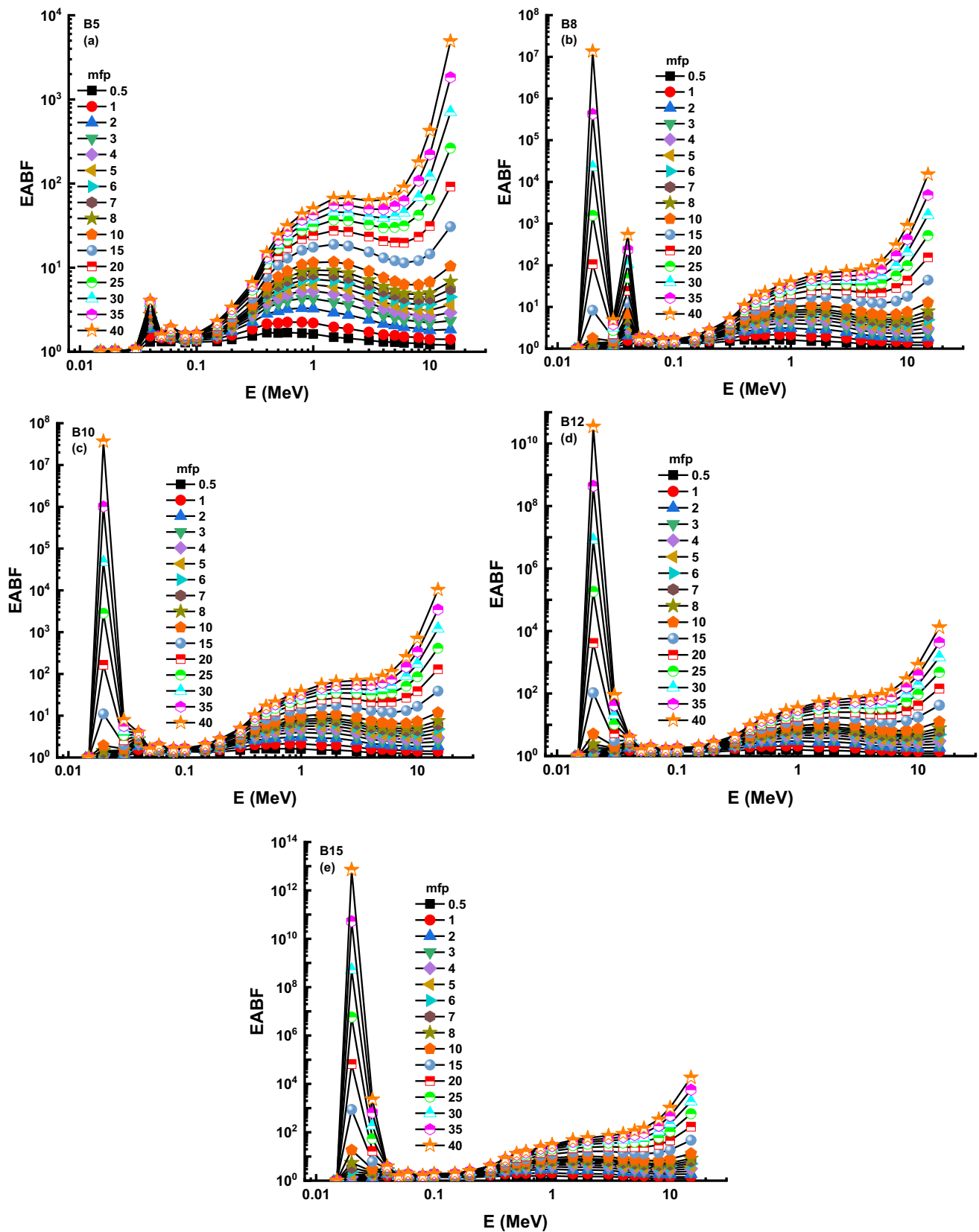
Fig. 9 Variation of energy absorption buildup factor (EABF) values of glasses at different MFP values (from 0.5 to 40MFP) as a function of incident photon energy (MeV)

TeO_2–ZnO–TiO_2–Na_2O–Bi_2O_3 chemical structure were investigated in a wide range of gamma-ray energy, i.e., from 0.015 to 15 MeV. As can be observed from the chemical compositions of the glasses, the amount of Bi_2O_3 reinforcement has been raised from 5 to 15% mole, while the quantity of TeO_2 reinforcement has been lowered from 75 to 65% (see Table 1). Meanwhile, the adjustment described above resulted in an increase in the glass density from 5.401 to 6.138 g/cm³. Figure 3 shows the variation of glass densities. One can say that 10% mole increment of Bi_2O_3 in the glass composition resulted in a 0.737 g/cm³ total improvement in the glass density. Following the understanding of density change in the glass structures, we have utilized a detailed characterization using a well-known online platform, namely Phy-X/PSD [31], in terms of determining some fundamental gamma-ray shielding parameters, namely mass attenuation coefficients (μ_m), half-value layer ($T_{0.5}$), mean free path (λ), effective atomic number (Z_{eff}), exposure buildup (EBF), and energy absorption buildup factors (EABF), respectively. Figure 4 depicts the variation of mass attenuation coefficients (cm²/g) of investigated glasses as an incident photon energy (MeV) function. As it is seen from the figure, there is a sharp

decrement in the low energy region, where the photo electric effect (PE) dominates all the photon–matter interactions. In the mid-energy region, the decrement was smoother than the low-energy region. This can be explained by the impact of Compton scattering (SC). However, the findings suggested that the B15 sample with the highest Bi_2O_3 content had the maximum μ_m vales across all photon energies examined. Due to the fact that μ_m is a density-independent parameter [36, 37], we may explain the preceding result in terms of elemental substitution between TiO_2 and Bi_2O_3. The rising Bi_2O_3 content also boosted the glass sample's total atomic weight from B5 to B15. As a result, the μ_m values of the glasses under examination significantly improved. On the other side, radiation protection studies need a thorough evaluation of the candidate shield materials used in radiation facilities in terms of determining the thickness, which may halve the intensity of incoming radiation. This is referred to as the half-value layer, and it is of considerable importance not only for radiation shielding investigations but also for medical diagnostic applications involving various modalities such as mammography. In this study, we determined the half-value layers of the glasses in a wide photon energy

Table 3 (EBF and EABF) G–P fitting coefficients (b, c, a, X_k, and d) of B5 sample

Energy (MeV)	Z_{eq}	G–P fitting parameters for EBF					G–P fitting parameters for EABF				
		a	b	c	d	X_k	a	b	c	d	X_k
0.015	26.24	−0.534	1.004	1.601	0.344	6.065	−0.534	1.004	1.601	0.344	6.065
0.020	28.06	0.720	1.010	0.111	−0.927	10.964	0.405	1.007	0.238	−0.445	14.306
0.030	28.51	0.203	1.021	0.361	−0.092	14.692	0.248	1.019	0.362	−0.179	12.443
0.040	44.07	0.090	3.840	0.570	−0.058	24.184	0.102	1.536	0.580	−0.040	20.487
0.050	44.48	−0.120	3.234	0.187	−0.041	13.555	−0.011	1.467	0.197	0.003	11.062
0.060	44.77	0.688	2.605	0.088	−0.114	12.926	0.477	1.415	0.109	−0.101	17.207
0.080	45.17	0.785	1.722	0.026	−0.213	14.838	0.640	1.339	0.061	−0.228	14.123
0.100	51.86	0.680	1.417	0.051	−0.279	13.977	0.654	1.369	0.062	−0.305	13.653
0.150	52.73	0.312	1.209	0.289	−0.176	13.865	0.477	1.434	0.152	−0.257	13.815
0.200	53.24	0.183	1.229	0.476	−0.098	14.419	0.359	1.573	0.249	−0.208	13.882
0.300	53.88	0.120	1.350	0.609	−0.057	14.007	0.243	1.855	0.395	−0.138	13.660
0.400	54.26	0.079	1.459	0.741	−0.047	14.128	0.181	2.148	0.526	−0.124	13.864
0.500	54.52	0.054	1.529	0.826	−0.038	14.086	0.128	2.191	0.647	−0.094	13.877
0.600	54.69	0.036	1.569	0.887	−0.029	13.876	0.102	2.252	0.715	−0.080	13.716
0.800	54.87	0.019	1.616	0.953	−0.022	13.785	0.069	2.251	0.809	−0.062	13.616
1.000	54.96	0.010	1.625	0.989	−0.021	13.293	0.053	2.197	0.861	−0.054	13.522
1.500	54.02	−0.014	1.551	1.092	−0.008	13.911	0.024	1.970	0.969	−0.039	13.589
2.000	51.35	−0.012	1.555	1.095	−0.011	13.096	0.026	1.877	0.971	−0.044	13.161
3.000	47.21	0.003	1.534	1.060	−0.032	12.941	0.043	1.715	0.935	−0.066	13.250
4.000	45.34	0.016	1.490	1.028	−0.044	13.391	0.058	1.593	0.899	−0.080	13.573
5.000	44.36	0.046	1.510	0.947	−0.071	13.621	0.087	1.566	0.830	−0.106	13.814
6.000	43.80	0.057	1.493	0.924	−0.081	13.844	0.099	1.514	0.807	−0.117	14.024
8.000	43.10	0.079	1.530	0.883	−0.098	14.151	0.111	1.480	0.795	−0.125	14.297
10.000	42.73	0.058	1.502	0.972	−0.078	14.207	0.087	1.413	0.882	−0.102	14.344
15.000	42.47	0.034	1.574	1.124	−0.060	14.144	0.063	1.406	1.022	−0.085	14.268

range. Half-value layer has an inverse correlation with any shielding material's linear attenuation coefficients. In other words, shielding materials having a greater number of linear attenuation coefficients may be referred to by their layer thicknesses with a lower half value. Thus, by demonstrating their superiority in gamma-ray attenuation, materials with lower half-value layers may halve the incoming gamma-ray intensity with smaller material thicknesses. In the current investigation, we determined the half-value layers of the glasses in the photon energy range of 0.015–15 MeV [37, 38, 39, 40]. Figure 5 shows the changes of half-value layer (cm) values of investigated glasses as a function of incident photon energy (MeV) and increasing Bi_2O_3 contribution in the glass structures (i.e., from 5 to 15% mole). The findings showed that B15 samples have the minimum half-value layer values at all photon energies. This is another clear example of the enhanced shielding qualities and the beneficial effect of increasing the quantity of Bi_2O_3 on the gamma-ray attenuation properties. The mean free part (λ) is a vital quantity in radiation sciences, notably in radiation shielding research. This is because the findings of provide unique knowledge in terms of a more accurate assessment

of the mean distance for an incident gamma-ray interaction with the material environment. As a conclusion, one may propose that dropping the value results in a more attenuating environment for energetic gamma-rays. We measured the values of all the glass samples examined in this study. The shifting tendency in the mean free path (λ) values of the investigated glasses as a function of incoming photon energy and increasing Bi_2O_3 contribution is shown in Fig. 6. We noticed that the shortest λ values are given for the B15 sample, which is consistent with the sample's smallest mean distance for adjacent gamma-ray interactions. It is necessary to assess an appropriate gamma-ray shield with a high effective atomic number. This is because the Z number of an element is related to the number of electrons in its atomic orbit. Given the critical role of electrons in orbit in interacting with gamma photons, it is predicted that elements or compounds with a high Z atomic number would have a greater number of electrons in orbit engagements. Given that increasing contact results in increased photon attenuation, a higher Z_{eff} value may be interpreted as another indicator of improved gamma-ray attenuation capabilities. As seen in Fig. 7, B15 has the highest Z_{eff} value of all gamma-ray energies. Additionally,

Table 4 (EBF and EABF) G–P fitting coefficients (b, c, a, X_k, and d) of B8 sample

Energy (MeV)	Z_{eq}	G–P fitting parameters for EBF					G–P fitting parameters for EABF				
		a	b	c	d	X_k	a	b	c	d	X_k
0.015	28.18	−0.374	1.002	1.917	0.278	9.696	−0.374	1.002	1.917	0.278	9.696
0.020	30.58	0.658	1.230	0.378	−0.911	11.140	0.382	1.038	0.490	−0.438	13.401
0.030	30.98	0.188	1.488	0.490	−0.081	15.597	0.222	1.106	0.500	−0.167	14.252
0.040	45.92	0.093	3.753	0.783	−0.080	24.881	0.097	1.577	0.802	−0.035	18.148
0.050	46.20	0.009	3.316	0.285	−0.104	14.604	0.083	1.523	0.292	−0.075	12.878
0.060	46.42	0.454	2.716	0.136	−0.095	10.337	0.296	1.465	0.157	−0.051	18.502
0.080	46.73	0.794	1.751	0.023	−0.193	15.043	0.671	1.357	0.052	−0.228	14.162
0.100	55.97	0.665	1.460	0.041	−0.188	14.367	0.643	1.437	0.047	−0.193	14.159
0.150	56.84	0.359	1.195	0.238	−0.205	13.744	0.546	1.429	0.111	−0.287	13.752
0.200	57.36	0.197	1.192	0.447	−0.105	14.199	0.399	1.516	0.208	−0.229	13.836
0.300	58.00	0.133	1.297	0.575	−0.063	13.835	0.278	1.786	0.340	−0.159	13.516
0.400	58.38	0.089	1.396	0.704	−0.051	14.143	0.207	2.038	0.471	−0.138	13.843
0.500	58.65	0.064	1.465	0.788	−0.041	14.112	0.151	2.082	0.591	−0.106	13.873
0.600	58.82	0.046	1.509	0.847	−0.032	13.794	0.118	2.128	0.667	−0.087	13.696
0.800	59.02	0.028	1.563	0.915	−0.025	13.669	0.083	2.166	0.763	−0.068	13.607
1.000	59.11	0.017	1.578	0.960	−0.022	13.328	0.066	2.140	0.819	−0.060	13.524
1.500	58.32	−0.007	1.530	1.062	−0.012	13.713	0.040	1.986	0.917	−0.050	13.568
2.000	56.23	0.000	1.553	1.051	−0.021	13.082	0.050	1.973	0.897	−0.064	13.299
3.000	52.72	0.010	1.531	1.038	−0.038	13.152	0.065	1.793	0.875	−0.087	13.359
4.000	50.88	0.019	1.477	1.026	−0.047	13.471	0.069	1.613	0.875	−0.092	13.668
5.000	49.90	0.046	1.490	0.957	−0.073	13.689	0.092	1.558	0.825	−0.113	13.889
6.000	49.33	0.059	1.480	0.932	−0.084	13.912	0.107	1.513	0.797	−0.127	14.092
8.000	48.64	0.077	1.526	0.907	−0.098	14.158	0.112	1.477	0.807	−0.129	14.332
10.000	48.27	0.050	1.504	1.019	−0.072	14.186	0.085	1.417	0.907	−0.104	14.302
15.000	47.95	0.028	1.587	1.186	−0.057	13.970	0.060	1.411	1.067	−0.088	14.136

Table 5 (EBF and EABF) G–P fitting coefficients (b, c, a, X_k and d) of B10 sample

Energy (MeV)	Z_{eq}	G–P fitting parameters for EBF					G–P fitting parameters for EABF				
		a	b	c	d	X_k	a	b	c	d	X_k
0.015	27.81	−0.404	1.002	1.858	0.291	9.012	−0.404	1.002	1.858	0.291	9.012
0.020	30.67	0.652	1.244	0.395	−0.902	11.162	0.378	1.040	0.505	−0.434	13.448
0.030	31.21	0.186	1.539	0.504	−0.084	15.987	0.219	1.115	0.514	−0.166	14.575
0.040	44.04	0.090	3.841	0.567	−0.057	24.173	0.102	1.536	0.576	−0.040	20.526
0.050	44.42	−0.125	3.230	0.183	−0.038	13.514	−0.015	1.465	0.193	0.006	10.990
0.060	44.69	0.700	2.599	0.086	−0.115	13.058	0.486	1.413	0.106	−0.104	17.141
0.080	45.08	0.785	1.721	0.027	−0.214	14.826	0.638	1.338	0.062	−0.228	14.121
0.100	56.32	0.663	1.463	0.041	−0.181	14.399	0.642	1.442	0.045	−0.184	14.200
0.150	57.37	0.367	1.194	0.231	−0.209	13.745	0.556	1.431	0.106	−0.290	13.765
0.200	58.00	0.200	1.189	0.441	−0.107	14.197	0.408	1.513	0.202	−0.233	13.828
0.300	58.75	0.134	1.288	0.571	−0.063	13.832	0.283	1.769	0.333	−0.161	13.498
0.400	59.22	0.091	1.385	0.699	−0.051	14.156	0.212	2.014	0.462	−0.140	13.834
0.500	59.52	0.066	1.453	0.781	−0.042	14.119	0.157	2.072	0.577	−0.109	13.869
0.600	59.72	0.048	1.497	0.839	−0.033	13.786	0.121	2.101	0.658	−0.089	13.690
0.800	59.96	0.030	1.552	0.907	−0.025	13.673	0.086	2.146	0.753	−0.070	13.606
1.000	60.05	0.018	1.568	0.954	−0.022	13.366	0.068	2.125	0.810	−0.061	13.521
1.500	59.12	−0.005	1.524	1.057	−0.013	13.756	0.041	1.974	0.913	−0.051	13.584
2.000	56.51	0.001	1.553	1.048	−0.022	13.081	0.052	1.978	0.893	−0.065	13.307
3.000	52.03	0.009	1.529	1.043	−0.037	13.111	0.061	1.773	0.887	−0.083	13.337
4.000	49.67	0.016	1.471	1.035	−0.045	13.427	0.063	1.586	0.892	−0.086	13.635
5.000	48.41	0.046	1.495	0.954	−0.072	13.671	0.091	1.560	0.826	−0.111	13.870
6.000	47.69	0.058	1.484	0.930	−0.083	13.893	0.105	1.513	0.800	−0.124	14.073
8.000	46.82	0.078	1.527	0.900	−0.098	14.156	0.112	1.478	0.803	−0.128	14.321
10.000	46.37	0.053	1.503	1.004	−0.074	14.193	0.086	1.416	0.898	−0.103	14.316
15.000	45.98	0.030	1.583	1.164	−0.058	14.030	0.061	1.410	1.051	−0.087	14.181

Table 6 (EBF and EABF) G–P fitting coefficients (b, c, a, X_k, and d) of B12 sample

Energy (MeV)	Z_{eq}	G–P fitting parameters for EBF						G–P fitting parameters for EABF				
		a	b	c	d	X_k		a	b	c	d	X_k
0.015	28.33	−0.363	1.002	1.940	0.274	9.953		−0.363	1.002	1.940	0.274	9.953
0.020	31.56	0.595	1.362	0.542	−0.822	11.355		0.346	1.056	0.644	−0.395	13.873
0.030	32.09	0.179	1.737	0.559	−0.097	17.504		0.208	1.153	0.570	−0.161	15.838
0.040	44.03	0.090	3.842	0.565	−0.057	24.169		0.102	1.535	0.575	−0.040	20.540
0.050	44.39	−0.127	3.229	0.182	−0.037	13.499		−0.016	1.464	0.192	0.008	10.965
0.060	44.66	0.704	2.597	0.085	−0.115	13.106		0.490	1.412	0.105	−0.105	17.117
0.080	45.05	0.785	1.720	0.027	−0.214	14.822		0.637	1.337	0.062	−0.228	14.120
0.100	57.78	0.582	1.487	0.063	−0.140	15.035		0.564	1.475	0.066	−0.140	14.762
0.150	58.87	0.392	1.195	0.212	−0.221	13.765		0.585	1.440	0.095	−0.295	13.825
0.200	59.52	0.208	1.181	0.427	−0.111	14.193		0.428	1.506	0.187	−0.242	13.810
0.300	60.30	0.137	1.272	0.563	−0.064	13.825		0.293	1.735	0.319	−0.167	13.462
0.400	60.77	0.094	1.363	0.689	−0.052	14.181		0.222	1.969	0.445	−0.146	13.816
0.500	61.08	0.070	1.432	0.768	−0.043	14.130		0.168	2.054	0.554	−0.115	13.862
0.600	61.28	0.052	1.476	0.824	−0.034	13.772		0.127	2.054	0.641	−0.091	13.679
0.800	61.53	0.033	1.534	0.893	−0.026	13.680		0.092	2.113	0.737	−0.072	13.603
1.000	61.62	0.020	1.551	0.944	−0.022	13.429		0.073	2.102	0.795	−0.064	13.517
1.500	60.72	−0.002	1.515	1.045	−0.015	13.842		0.042	1.950	0.906	−0.051	13.616
2.000	58.18	0.002	1.543	1.044	−0.022	13.092		0.055	1.969	0.882	−0.067	13.329
3.000	53.64	0.012	1.534	1.032	−0.039	13.205		0.071	1.819	0.859	−0.092	13.388
4.000	51.18	0.020	1.479	1.023	−0.048	13.485		0.072	1.622	0.869	−0.094	13.677
5.000	49.84	0.046	1.491	0.957	−0.073	13.688		0.092	1.558	0.825	−0.113	13.888
6.000	49.08	0.059	1.481	0.932	−0.084	13.909		0.107	1.513	0.798	−0.126	14.089
8.000	48.15	0.077	1.526	0.905	−0.098	14.158		0.112	1.478	0.806	−0.128	14.329
10.000	47.66	0.051	1.503	1.014	−0.073	14.188		0.086	1.417	0.904	−0.103	14.306
15.000	47.23	0.029	1.586	1.178	−0.058	13.992		0.060	1.411	1.061	−0.087	14.152

Table 7 (EBF and EABF) G–P fitting coefficients (b, c, a, X_k, and d) of B15 sample

Energy (MeV)	Z_{eq}	G–P fitting parameters for EBF					G–P fitting parameters for EABF				
		a	b	c	d	X_k	a	b	c	d	X_k
0.015	29.01	−0.309	1.001	2.042	0.252	11.152	−0.309	1.001	2.042	0.252	11.153
0.020	32.75	0.521	1.516	0.734	−0.717	11.607	0.304	1.078	0.825	−0.345	14.424
0.030	33.27	0.169	1.993	0.631	−0.113	19.471	0.195	1.201	0.641	−0.156	17.473
0.040	44.01	0.090	3.842	0.564	−0.057	24.163	0.102	1.535	0.573	−0.040	20.560
0.050	44.36	−0.130	3.228	0.180	−0.036	13.478	−0.018	1.463	0.190	0.009	10.928
0.060	44.62	0.710	2.594	0.084	−0.116	13.173	0.495	1.411	0.104	−0.106	17.083
0.080	45.00	0.784	1.719	0.027	−0.215	14.816	0.636	1.337	0.062	−0.228	14.119
0.100	59.71	0.393	1.529	0.120	−0.075	16.415	0.380	1.529	0.121	−0.077	15.918
0.150	60.86	0.424	1.196	0.187	−0.237	13.791	0.622	1.450	0.081	−0.302	13.903
0.200	61.52	0.217	1.171	0.410	−0.116	14.187	0.455	1.496	0.167	−0.253	13.787
0.300	62.31	0.140	1.250	0.552	−0.065	13.817	0.306	1.692	0.301	−0.173	13.417
0.400	62.79	0.097	1.337	0.676	−0.053	14.212	0.233	1.912	0.424	−0.152	13.793
0.500	63.10	0.074	1.405	0.751	−0.044	14.144	0.181	2.032	0.524	−0.123	13.854
0.600	63.31	0.056	1.451	0.806	−0.035	13.756	0.135	1.996	0.621	−0.094	13.665
0.800	63.55	0.037	1.511	0.876	−0.028	13.688	0.099	2.071	0.716	−0.075	13.601
1.000	63.66	0.023	1.530	0.931	−0.022	13.507	0.079	2.072	0.775	−0.066	13.511
1.500	62.80	0.001	1.502	1.031	−0.016	13.950	0.045	1.920	0.896	−0.052	13.657
2.000	60.36	0.002	1.525	1.043	−0.021	13.115	0.057	1.936	0.876	−0.068	13.345
3.000	55.77	0.017	1.540	1.017	−0.043	13.324	0.085	1.877	0.823	−0.104	13.453
4.000	53.25	0.026	1.495	1.004	−0.053	13.579	0.086	1.686	0.832	−0.106	13.741
5.000	51.81	0.053	1.523	0.938	−0.077	13.763	0.106	1.639	0.791	−0.126	13.950
6.000	50.99	0.062	1.505	0.926	−0.085	13.961	0.114	1.560	0.783	−0.132	14.126
8.000	50.02	0.076	1.526	0.913	−0.098	14.160	0.112	1.479	0.810	−0.129	14.340
10.000	49.48	0.049	1.504	1.029	−0.071	14.182	0.085	1.418	0.912	−0.104	14.294
15.000	48.99	0.027	1.590	1.197	−0.057	13.939	0.059	1.412	1.075	−0.088	14.112

as compared to the other glasses investigated, this condition is related with the greatest Bi ($Z=83$) concentration in B15. Backscattering or photon reflection is a serious issue for researchers and suppliers of gamma-ray protection. It is a primary challenge in radiation shielding. As a response, successful geometry design is seen as a significant obstacle in this area. The buildup factor plays an important role for correct gamma attenuation measurements and may impact measurement precision. When gamma radiation travels through shielding substance, two different types of radiation are produced: un-collided photons and collided photons. As a conclusion, the accumulation factor is an essential statistic for determining the presence of gamma-rays. It is calculated as the proportion of total particles at a point to total particles that have not collided at that location. The shields with the lowest exposure (EBF) and energy absorption (EABF) buildup factors among the examined materials may be classified outstanding shielding substances. The exposure (EBF) and energy absorption (EABF) buildup factors of B5, B8, B10, B12, and B15 glasses were measured in this research. Figures 8 and 9 illustrate how the exposure buildup factor (EBF) and energy absorption buildup factor (EABF) values

of glasses evolve as a function of incoming photon energy at various mfp values (from 0.5 to 40 mfp) (MeV). The (EBF and EABF) G–P fitting coefficients (b, c, a, X_k, and d) of B5–B15 samples are shown in Tables 3, 4, 5, 6 and 7. As can be seen, the EBF and EABF values decrease from B5 to B15, demonstrating that the shielding enhancement of glass samples has strengthened. On the other hand, changes in behavior in three photon–matter interaction domains were observed, namely low, medium, and high energy, as a result of the photoelectric effect, Compton scattering, and pair creation, respectively. Our findings suggested that the B15 sample has the lowest EBF and EBF values of all the glass samples examined.

Conclusion

The objectives of this work are to explore the optical properties and gamma-ray attenuation competencies of bismo-tellurite sodium titanium zinc glass samples with chemical

formula $(80 - x)TeO_2–10ZnO–5TiO_2–5Na_2O–xBi_2O_3$, where $x = 5, 8, 10, 12,$ and 15 mol%. Our findings revealed that:

1- Values of optical electronegativity (χ^*) were varied from 0.715 for B5 glass sample to 0.677 for B15 glass sample.
2- Values of linear dielectric susceptibility ($\chi^{(1)}$) were varied from 0.400 for B5 glass sample to 0.430 for the glass sample.
3- Values of non-linear optical susceptibility (χ^3) and non-linear refractive index ($n_2^{optical}$) were varied from 4.379×10^{-12} to 5.812×10^{-12} (esu) and from 6.719×10^{11} to 8.656×10^{-11} (esu) for B5 and B15 glasses, respectively.
4- The B15 sample with the highest Bi_2O_3 content had the maximum mass attenuation coefficient (μ_m) values across all examined photon energies, while B5 sample with the lowest Bi_2O_3 content had the minimum (μ_m).
5- Both half-value layer ($T_{0.5}$) and mean free path (λ) followed the trend as follows: $(T_{0.5}, \lambda)_{B5} > (T_{0.5}, \lambda)_{B8} > (T_{0.5}, \lambda)_{B10} > (T_{0.5}, \lambda)_{B12} > (T_{0.5}, \lambda)_{B15}$.
6- The EBF and EABF values decrease from B5 to B15, demonstrating that the shielding enhancement of glass samples has strengthened.
7- The effective atomic number (Z_{eff}) parameter followed the trend as follows: $(Z_{eff})_{B15} > (Z_{eff})_{B12} > (Z_{eff})_{B10} > (Z_{eff})_{B8} > (Z_{eff})_{B5}$.

Our findings confirm that the enhancement of Bi_2O_3 content in the bismo-tellurite sodium titanium zinc glass samples play an important role of improvement both optical and gamma-ray protection properties.

Author contribution All authors wrote the first draft of the manuscript. All authors edited the manuscript and approved the final version.

Data Availability Statements and Author Contribution All authors contribute in Conceptualization, Methodology, Software, Validation, Investigation, Data Curation, Writing-Review and Editing, Visualization

Declarations

Ethics approval The authors declare that this manuscript is original, has not been published before, and is not currently being considered for publication elsewhere.

Consent to participate The authors consent to participate.

Consent for publication The author's consent for publication.

Competing interests The authors declare no competing interests.

References

1. Kara, U., Susoy, G., Issa, S.A.M., Elshami, W., Yorgun, N.Y., Abuzaid, M.M., Kavaz, E., Tekin, H.O.: Iron (III) oxide doped lithium borate glasses: structural and charged particles/photon shielding properties. J. Non. Cryst. Solids. **546**, 120281 (2020). https://doi.org/10.1016/J.JNONCRYSOL.2020.120281

2. Rammah, Y.S., Olarinoye, I.O., El-Agawany, F.I., Yousef, E.S., Ibrahim, S., Ali, A.A.: SrO-reinforced potassium sodium borophosphate bioactive glasses: compositional, physical, spectral, structural properties and photon attenuation competence. J. Non. Cryst. Solids. **559**, 120667 (2021). https://doi.org/10.1016/J.JNONCRYSOL.2021.120667

3. Rammah, Y.S., Sayyed, M.I., El-bashir, B.O., Asiri, S.M., Al-Hadeethi, Y.: Linear optical features and radiation shielding competence of ZnO–B2O3–TeO2-Eu2O3 glasses: role of Eu3+ ions. Opt. Mater. (Amst). **111**, 110525 (2021). https://doi.org/10.1016/J.OPTMAT.2020.110525

4. Zakaly, H.M.H., Saudi, H.A., Tekin, H.O., Rashad, M., Issa, S.A.M., Rammah, Y.S., Elazaka, A.I., Hessien, M.M., Ene, A.: Glass fabrication using ceramic and porcelain recycled waste and lithium niobate: physical, structural, optical and nuclear radiation attenuation properties. J. Mater. Res. Technol. **15**, 4074–4085 (2021). https://doi.org/10.1016/J.JMRT.2021.09.138

5. El-Denglawey, A., Zakaly, H.M.H., Alshammari, K., Issa, S.A.M., Tekin, H.O., AbuShanab, W.S., Saddeek, Y.B.: Prediction of mechanical and radiation parameters of glasses with high Bi2O3 concentration. Results. Phys. **21**, 103839 (2021). https://doi.org/10.1016/j.rinp.2021.103839

6. Mostafa, A.M.A., Zakaly, H.M.H., Pyshkina, M., Issa, S.A.M., Tekin, H.O., Sidek, H.A.A., Matori, K.A., Zaid, M.H.M.: Multi-objective optimization strategies for radiation shielding performance of BZBB glasses using Bi2O3: a FLUKA Monte Carlo code calculations. J. Mater. Res. Technol. **9**, 12335–12345 (2020). https://doi.org/10.1016/j.jmrt.2020.08.077

7. G. Almisned, HO., Tekin, A., Ene, SAM., Issa, G., Kilic, HMH., Zakaly, A. closer look on nuclear radiation shielding properties of Eu3+ doped heavy metal oxide glasses: impact of Al2O3/PbO substitution, Mater. 2021. **14**, 5334 (2021). https://doi.org/10.3390/MA14185334

8. Abouhaswa, A.S., Zakaly, H.M.H., Issa, S.A.M., Rashad, M., Pyshkina, M., Tekin, H.O., El-Mallawany, R., Mostafa, M.Y.A.: Synthesis, physical, optical, mechanical, and radiation attenuation properties of TiO2–Na2O–Bi2O3–B2O3 glasses. Ceram. Int. **47**, 185–204 (2021). https://doi.org/10.1016/j.ceramint.2020.08.122

9. Mahmoud, I.S., Issa, S.A.M., Zakaly, H.M.H., Saudi, H.A., Ali, A.S., Saddeek, Y.B., Alharbi, T., Tekin, H.O.: Material characterization of WO3/Bi2O3 substituted calcium-borosilicate glasses: structural, physical, mechanical properties and gamma-ray resistance competencies. J. Alloys Compd. **888**, 161419 (2021). https://doi.org/10.1016/j.jallcom.2021.161419

10. Hivrekar, M.M., Bhoyar, D.N., Mande, V.K., Dhole, V.V., Solunke, M.B., Jadhav, K.M.: Effect of RE (Nd3+, Sm3+) oxide on structural, optical properties of Na2O-Li2O-ZnO-B2O3 glass system. AIP Conf. Proc. **1953**, 090074 (2018). https://doi.org/10.1063/1.5032921

11. Đô, P.V.: Sm3+ doped borotellurite glass: absorption, fluorescence and optical parameters. VNU. J. Sci. Math. Phys. **34**, 33–39 (2018). https://doi.org/10.25073/2588-1124/VNUMAP.4258

12. Marzouk, M.A., ElBatal, H.A., Ghany, A.A., Eldin, F.E.: Ultraviolet, visible, ESR, and infrared spectroscopic studies of CeO2-doped lithium phosphate glasses and effect of gamma irradiation. J. Mol. Struct. **997**(1–3), 94–102 (2011)

13. Menazea, A.A., Abdelghany, A.M., Hakeem, N.A., Osman, W.H., El-kader, A.: Precipitation of silver nanoparticles in borate glasses by 1064 nm Nd: YAG nanosecond laser pulses: characterization and dielectric studies. J. Electron. Mater. **49**(1), 826–832 (2020)

14. Ibrahim, A.M., Hammad, A.H., Abdelghany, A.M., Rabie, G.O.: Mixed alkali effect and samarium ions effectiveness on the structural, optical and non-linear optical properties of borate glass. J. Non-Cryst. Solids **495**, 67–74 (2018)

15. Abdelghany, A.M., ElBatal, H.A.: Effect of TiO2 doping and gamma ray irradiation on the properties of SrO–B2O3 glasses. J. Non-Cryst. Solids **379**, 214–219 (2013)

16. Mortada, W.I., Kenawy, I.M., Abdelghany, A.M., Ismail, A.M., Donia, A.F., Nabieh, K.A.: Determination of Cu2+, Zn2+ and Pb2+ in biological and food samples by FAAS after preconcentration with hydroxyapatite nanorods originated from eggshell. Mater. Sci. Eng. C **52**, 288–296 (2015)

17. Shaalan, M., El-Damrawi, G., Hassan, A., Misbah, M.H.: Structural role of Nd2O3 as a dopant material in modified borate glasses and glass ceramics. J. Mater. Sci. Mater. Electron. **32**, 12348–12357 (2021). https://doi.org/10.1007/S10854-021-05866-X/FIGURES/7

18. Misbah, M.H., Doweidar, H., Ramadan, R., El-Kemary, M.: Tailoring the structure and properties of iron oxide nanoparticles through the oxygen species of borate glass matrix. J. Non. Cryst. Solids. **545**, 120241 (2020). https://doi.org/10.1016/J.JNONCRYSOL.2020.120241

19. J. Kim, N. Wang, Y. Chen, al -, Z. Zhu, G. Zheng, R. Zhang, F. Marchini, F.J. Williams, E.J. Calvo -, M.S. Meikhail, I.A. Gohar, A.A. Megahed, Lithium borosilicate glasses as electrolyte for solid state batteries, J. Phys. D. Appl. Phys. **26** (1993) 1125. https://doi.org/10.1088/0022-3727/26/7/019.

20. Tatsumisago, M., Takano, R., Nose, M., Nagao, K., Kato, A., Sakuda, A., Tadanaga, K., Hayashi, A.: Electrical and mechanical properties of glass and glass-ceramic electrolytes in the system Li3BO3–Li2SO4. J. Ceram. Soc. Japan. **125**, 433–437 (2017). https://doi.org/10.2109/JCERSJ2.17026

21. Ravangvong, S., Chanthima, N., Rajaramakrishna, R., Kim, H.J., Sangwaranatee, N., Kaewkhao, J.: Dy3+ ions doped (Na2O/NaF)-Gd2O3–P2O5 glasses for solid state lighting material applications. Solid. State. Sci. **97**, 105972 (2019). https://doi.org/10.1016/J.SOLIDSTATESCIENCES.2019.105972

22. E. Paweł Golis, M. Reben, J. Wasylak, J. Filipecki, Investigations of tellurite glasses for optoelectronics devices, Opt. Appl. XXXVIII (2008).

23. A.M.A.H. Y.S. Rammah, Hesham M.H. Zakaly, Shams A M Issa, H.O. Tekin, M.M. Hessien, H. A. Saudi, Fabrication, physical, structural, optical investigation of cadmium lead-borate glasses doped with Nd3+ ions: experimental study, J. Mater. Sci. Mater. Electron 33 (2022) 1877–1887.

24. Singh, V.P., Badiger, N.M., Kaewkhao, J.: Radiation shielding competence of silicate and borate heavy metal oxide glasses: comparative study. J. Non. Cryst. Solids. **404**, 167–173 (2014). https://doi.org/10.1016/J.JNONCRYSOL.2014.08.003

25. Misbah, M.H., Abdelghany, A.M., El-Agawany, F.I., Rammah, Y.S., El-Mallawany, R.: On Y2O3·Li2O·Al2O3·B2O3 glasses: synthesis, structure, physical, optical characteristics and gamma-ray shielding behavior. J. Mater. Sci. Mater. Electron. **32**, 16242–16254 (2021)

26. Olarinoye, I.O., El-Agawany, F.I., Gamal, A., Yousef, E.S., Rammah, Y.S.: Investigation of mechanical properties, photons, neutrons, and charged particles shielding characteristics of Bi2O3/B2O3/SiO2 glasses. Appl. Phys. A Mater. Sci. Process. **127**, 1–16 (2021)

27. Almatari, M., Agar, O., Altunsoy, E.E., Kilicoglu, O., Sayyed, M.I., Tekin, H.O.: Photon and neutron shielding characteristics of samarium doped lead alumino borate glasses containing barium, lithium and zinc oxides determined at medical diagnostic energies. Results. Phys. **12**, 2123–2128 (2019). https://doi.org/10.1016/j.rinp.2019.01.094

28. Agar, O., Tekin, H.O., Sayyed, M.I., Korkmaz, M.E., Culfa, O., Ertugay, C.: Experimental investigation of photon attenuation behaviors for concretes including natural perlite mineral. Results. Phys. **12**, 237–243 (2019). https://doi.org/10.1016/j.rinp.2018.11.053

29. Henaish, A., Issa, S.A.M., Zakaly, H.M., Tekin, H.O.O., Abouhaswa, A.S.: Characterization of optical and radiation shielding behaviors of ferric oxide reinforced bismuth borate glass. Phys. Scr. (2021). https://doi.org/10.1088/1402-4896/abf581

30. G. Almisned, H.O. Tekin, E. Kavaz, G. Bilal, S.A.M. Issa, H.M.H. Zakaly, A. Ene, Gamma, fast neutron, proton, and alpha shielding properties of borate glasses: a closer look on lead (II) oxide and bismuth (III) oxide reinforcement, Appl. Sci. 2021. **11**, 6837 (2021). https://doi.org/10.3390/APP11156837.

31. Şakar, E., Özpolat, Ö.F., Alım, B., Sayyed, M.I., Kurudirek, M.: Phy-X/PSD: development of a user friendly online software for calculation of parameters relevant to radiation shielding and dosimetry. Radiat. Phys. Chem. **166**, 108496 (2020). https://doi.org/10.1016/j.radphyschem.2019.108496

32. Fong, W.L., Bashar, K.A., Baki, S.O., Zaid, M.H.M., Goh, B.T., Mahdi, M.A.: Thermal, structural and optical properties of Bi2O3-Na2O-TiO2-ZnO-TeO2 glass system. J. Non. Cryst. Solids. **555**, 120621 (2021). https://doi.org/10.1016/J.JNONCRYSOL.2020.120621

33. J. A. Duffy, Bonding, energy level and bonds in inorganic, in: Longman Sci. Tech., Longman, England, 1990. https://scholar.google.com/scholar?hl=en&as_sdt=0%2C5&q=J.+A.+Duffy%2C+Bonding%2C+Energy+Level+and+Bonds+in+Inorganic+Solids+%28Longman%2C+England%2C+1990%29.&btnG. Accessed 16 December 2021).

34. M.D.-L.N. (Massachusetts I. of, undefined 2001, Solid state physics part II optical properties of solids, Yumpu.Com. (n.d.). https://www.yumpu.com/en/document/view/5491599/solid-state-physics-part-ii-optical-properties-of-solids (accessed December 16, 2021).

35. Tichá, H., Tichý, L.: Semiempirical relation between non-linear susceptibility (refractive index), linear refractive index and optical gap and its application to amorphous chalcogenides. J. Optoelectron. Adv. Mater. **4**, 381–386 (2002)

36. Zakaly, H.M., Ashry, A., El-Taher, A., Abbady, A.G.E., Allam, E.A., El-Sharkawy, R.M., Mahmoud, M.E.: Role of novel ternary nanocomposites polypropylene in nuclear radiation attenuation properties: in-depth simulation study. Radiat. Phys. Chem. **188**, 109667 (2021). https://doi.org/10.1016/j.radphyschem.2021.109667

37. Zakaly, H.M.H., Saudi, H.A., Issa, S.A.M., Rashad, M., Elazaka, A.I., Tekin, H.O., Saddeek, Y.B.: Alteration of optical, structural,

mechanical durability and nuclear radiation attenuation proper-
ties of barium borosilicate glasses through BaO reinforcement:
experimental and numerical analyses. Ceram. Int. **47**, 5587–5596
(2021). https://doi.org/10.1016/j.ceramint.2020.10.143

38. Tekin, H.O., Shams, A.M.I., Emad, M.A., Rammah, Y.S.: Lith-
ium-fluoro borotellurite glasses: nonlinear optical, mechanical,
characteristics and gamma radiation protection characteristics.
Radiat. Phys. Chem. **190**, 109819 (2022)

39. Rammah, Y.S., El-Agawany, F.I., Abdel Wahab, E.A., Hessien,
M.M., Shaaban, K.H.S.: Significant impact of V2O5 content
on lead phosphor-arsenate glasses for mechanical and radiation
shielding applications. Radiat. Phys. Chem. **193**, 109956 (2022)

40. Abdelghany, A.M., Rammah, Y.S.: Transparent alumino lithium
borate glass-ceramics: synthesis, structure and gamma-ray shield-
ing attitude. J. Inorg. Organomet. Polym Mater. **31**, 2560–2568
(2021)